Available online at www.sciencedirect.com
SCIENCE DIRECT®
Journal of the European Ceramic Society 25 (2005) 759–765
www.elsevier.com/locate/jeurceramsoc

Thermal annealing effects on the structural and electrical properties of PMN–PZ–PT ternary thin films deposited by a sol–gel process

Santiranjan Shannigrahi*, Kui Yao

Institute of Materials Research and Engineering (IMRE), 3 Research Link, Singapore 117602, Singapore

Received 14 January 2004; received in revised form 12 March 2004; accepted 24 March 2004

Available online 1 July 2004

Abstract

Thin film samples of 0.15PMN–0.45PZ–0.40PT (PMN–PZ–PT) three-component system were prepared on Pt-coated Si substrates by a sol–gel process. X-ray diffraction (XRD), scanning electron microscopy (SEM), transmission electron microscopy (TEM), atomic force microscopy (AFM), and secondary ion mass spectrometry (SIMS) show that the above films can be formed in a single-phase perovskite structure at 800 °C. This was further confirmed by the dielectric and ferroelectric properties of the samples annealed at different temperatures. It was demonstrated that the morphology and microstructures of the PMN–PZ–PT films were quite sensitive to their annealing conditions, which strongly affects their electrical properties.

Keywords: Sol–gel process; X-ray methods; Dielectric properties; Ferroelectric properties; Films; $PbTiO_3$

1. Introduction

Because of their high dielectric permittivity and piezoelectric properties, $Pb(Mg_{1/3}Nb_{2/3})O_3$ (PMN), $Pb(Zn_{1/3}Nb_{2/3})O_3$ (PZN) and their solid solutions with $PbTiO_3$ (PT), both bulk and thin film forms, are potentially promising candidates for various microelectromechanical systems (MEMS).[1–8] The interest in thin film is due to the growing need for miniaturized electromechanical actuators, transducers, and sensors in many fields of science and technology. Various fabrication methods are used for present day ferroelectric thin film fabrication, amongst which is a sol–gel method that appears to have one of the highest possibilities of controlling the stoichiometric composition.[9,10] However, sol–gel processed films involve repeated cycles of coating, followed by heat treatment, to achieve required thicknesses. To ensure suitable thin film properties, the materials should be dense, chemically homogeneous, and in a pure perovskite phase. Hence, optimization of the final annealing temperature is the most critical processing parameter.

In this article, we report the synthesis and characterization of $[0.15Pb(Mg_{1/3}Nb_{2/3})O_3–0.45PbZrO_3–0.40PbTiO_3]$ (hereafter PMN–PZ–PT) thin films deposited by a sol–gel technique. PMN–PZ–PT systems are currently attracting much attention in the research community, presumably due to their large piezoelectric coefficient that is most likely caused by the very large response of the internal coordinates of Pb, Ti, Zr, Nb, and O atoms to any macroscopic strain.[11] There are few reports within the literature on PMN–PZ–PT in both its film and ceramics forms.[12–15] Moreover, no systematic study of its perovskite phase-formation temperature during sol–gel processing has been made, and there are only reports of a broad range of annealing temperatures.[15] Thus, optimization of the perovskite formation temperature is required to improve such a system. With this in mind, we have prepared PMN–PZ–PT thin films through a sol–gel process, employing different annealing temperatures that have been optimized based on detailed structural and electrical characterizations.

2. Experimental methods

2.1. Thin film preparation

The precursor solution for the PMN–PZ–PT sol with the present composition $[0.15Pb(Mg_{1/3}Nb_{2/3})O_3–0.45PbZrO_3–0.40PbTiO_3]$ was prepared first by dissolving

* Corresponding author. Tel.: +65 6874 8299; fax: +65 6872 0785.
E-mail address: santi-s@imre.a-star.edu.sg (S. Shannigrahi).

0955-2219/$ – see front matter © 2004 Elsevier Ltd. All rights reserved.
doi:10.1016/j.jeurceramsoc.2004.03.030

appropriate amounts of lead acetate trihydrate [$(CH_3CO_2)_2$-$Pb{\cdot}3H_2O$], zirconium acetylacetonate [$CH_3COCH{=}C(O–)$-$CH_3]_4Zr$, and magnesium acetate tetrahydrate [$(CH_3CO_2)_2$-$Mg{\cdot}4H_2O$] in acetic acid at 105 °C in a vessel, and in another vessel appropriate amounts of titanium isopropoxide $\{Ti[OCH(CH_3)_2]_4\}$, and niobium ethoxide $[Nb(OC_2H_5)_5]$ were dissolved in 2-ethoxyethanol at room temperature. Finally the above two precursor solutions were mixed and refluxed for 3 h, which yielded clear sol. All manipulations were performed under dry nitrogen atmosphere inside a glove box. Acetylacetone and polyethylene glycol were added into the solution as a stabilizing and a drying control agent, respectively, which can result crack free films. To compensate for the loss of lead during annealing, an additional 10 mol% lead was incorporated to the precursor solution. Then, the sol was deposited onto $Pt/Ti/SiO_2/Si$ substrates by a spin coating at 5000 rpm for 20 s. Thereafter, Drying and pyrolysis steps in atmospheric air at 110 °C for 2 min and 430 °C for 5 min, respectively, were performed following each multilayer film coating. Finally, the multilayer films were annealed in atmospheric air at four different temperatures (700, 750, 800, and 850 °C) using a furnace, with a heating rate of 200 °C mm^{-1}. A short holding time of 1 min was employed for each film, so as to compare and optimize their structural and electrical properties.

2.2. Film characterization

Film structures were studied with a X-ray diffraction (XRD) system (D8-ADVANCE, Bruker AXS GmbH, Germany) using Cu Kα radiation ($\lambda = 0.15418$ nm) in a wide range of Bragg angle ($20° < 2\theta < 60°$) at room temperature. The surface morphology and thickness were characterized using scanning electron microscopy (SEM) (JSM-6700F, JEOL Ltd., Japan) operated at 10 kV and transmission electron microscopy (TEM) (Philips CM300) operated at 300 keV. Plan view specimens for TEM were prepared by a standard technique.[16] Average surface roughness was estimated using an atomic force microscopy (AFM) (Nanonics AFM NSOM 100, Israel), operating in tapping mode. Depth profile analyses were carried out using a secondary ion mass spectrometry (SIMS) (ION-ToF GmbH, ToF-SIMS IV).

Electrical characterizations were accomplished after Au electrodes were sputtered onto the films and a small corner area on each sintered film was wet etched in order to expose the Pt bottom electrode. A typical area of the top electrodes was 10^{-4} cm^2. Ferroelectric hysteresis loops were measured by using a RT66A (Radiant Technology). The dependence of the dielectric permittivity and loss tangent on the frequency was measured at room temperature using an Impedance/Gain-Phase Analyzer (HP 4194 A) and the room temperature leakage currents were measured using a Keithley electrometer (Model No. 236). The leakage current of the PMN–PZ–PT films was measured by applying a dc voltage of 0–5 V while the bottom electrode was grounded.

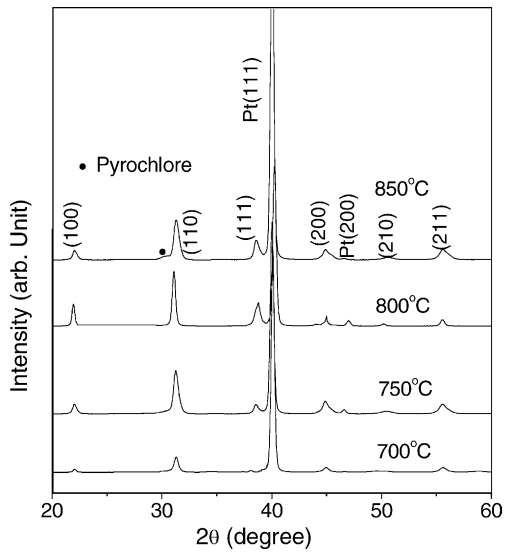

Fig. 1. Comparison of XRD of the PMN–PZ–PT films annealed at different temperatures.

3. Results and discussion

3.1. Structural study

Fig. 1 shows comparisons of the room temperature XRD patterns of the PMN–PZ–PT films sintered at different temperatures. The films annealed at 700 and 750 °C show poor crystallinity. The sharpest single-diffraction peaks correspond to the samples annealed at 800 °C, indicating better crystallization in the samples with a polycrystalline texture. A small pyrochlore phase, however, appeared in the films annealed at 850 °C. Finally, the polycrystalline film orientations ($h\,k\,l$) were indexed and the lattice parameters were determined and refined using a least-squares regression method in PowdMult.[17] A tetragonal unit cell was finally selected for every samples on the basis that it formed the best agreement between the calculated and observed interplanar spacings (d) of all diffraction lines and minimum $\sum \Delta d$, where $\sum \Delta d = \sum(d_{obs} - d_{cal})$. The interplanar spacings (d_{hkl}) for the films annealed at different temperatures, assessed from XRD data are given in Table 1. The calculated tetragonal cell parameters are $a = 0.40(29)$, 0.40(33), 0.40(36), and 0.40(31) nm and $c = 0.40(53)$, 0.40(60), 0.40(97), and 0.40(46) nm for the films annealed at 700, 750, 800, and 850 °C, respectively.

3.2. Surface morphology study

SEM micrographs for the different films are given in Fig. 2. The samples annealed at 700 °C contain sub-micron sized grains without any distinct coalescent grain structure. The grain coalescence structures appeared in the films annealed at 750 °C, in which some sub-micron sized grains coalesced to form grain clusters. With an increasing annealing temperature (800 °C), even more grain coalescent clusters

Table 1
Comparisons of observed *d*-values (nm) measured from XRD (d_{XRD}) of PMN–PZ–PT films annealed at different temperatures and that measured from TEM (d_{TEM}) of the films annealed at 800 °C

h	*k*	*l*	d_{XRD} (700 °C)	d_{XRD} (750 °C)	d_{XRD} (800 °C)	d_{XRD} (850 °C)	d_{TEM} (800 °C)
1	0	0	0.40(29)	0.40(33)	0.40(36)	0.40(31)	–
1	1	0	0.28(57)	0.28(61)	0.28(75)	0.28(56)	0.28(33)
1	1	1	0.23(60)	0.23(36)	0.23(26)	0.23(32)	0.23(24)
2	0	0	0.20(15)	0.20(26)	0.20(14)	0.20(18)	0.20(07)
2	1	0	–	0.18(10)	0.18(16)	0.18(08)	0.18(07)
2	1	1	0.16(53)	0.16(54)	0.16(54)	0.16(53)	–

appeared, and eventually grain clusters connected to each other. Such grain coalescence was enhanced further upon heating the samples to 850 °C.

However, at higher annealing temperatures, lead loss that resulted from evaporation and a lead-deficient pyrochlore phase appears, leading to degradation of the final perovskite film (Fig. 1). The reproducibility of the film features has been verified by characterizing at least two films prepared in exactly the same manner. The thicknesses were estimated to be around 1.7 μm.

Judging from their XRD and SEM analysis, we have selected the films annealed at 800 °C as optimal, which were then further analyzed by TEM. The microstructures are shown in Fig. 3(a). Pores are also observed in this image that appear due to the burnout of embedded organic polymer within the films. On the other hand, the presence of porosity

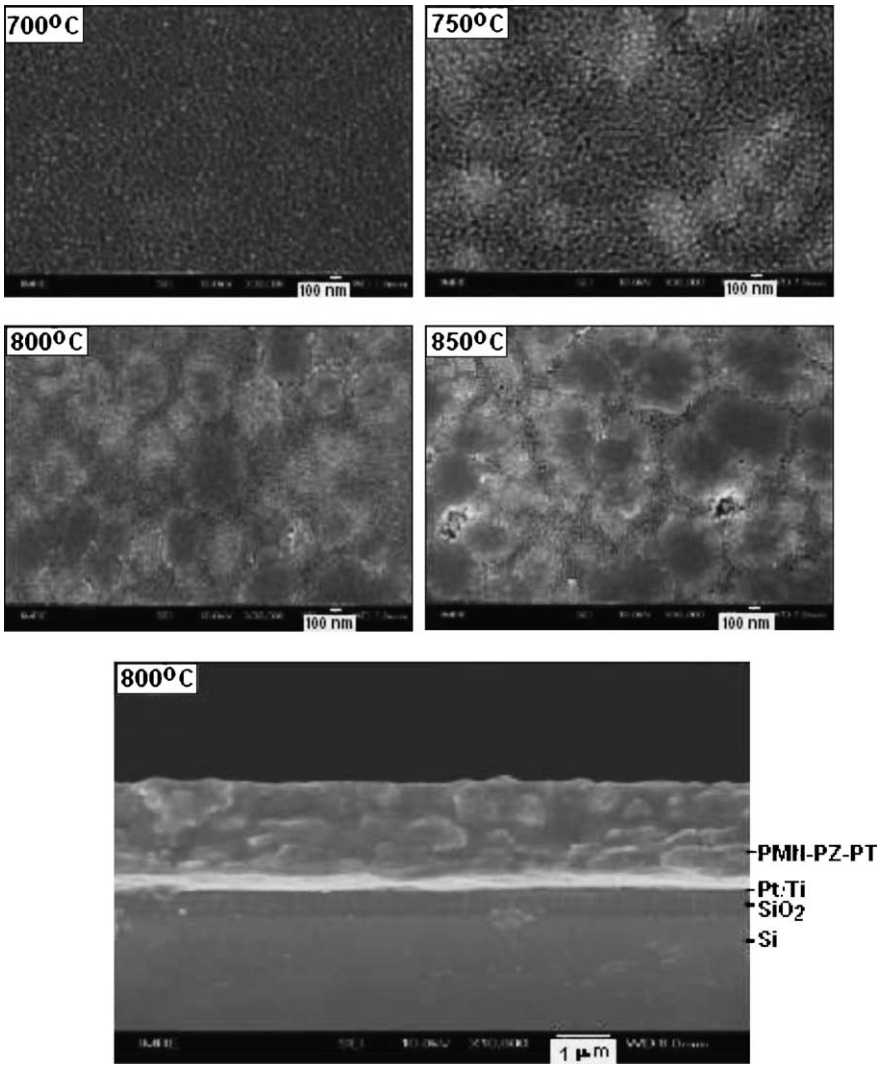

Fig. 2. SEM surface morphology of the PMN–PZ–PT films annealed at different temperatures and the cross-section of the film annealed at 800 °C.

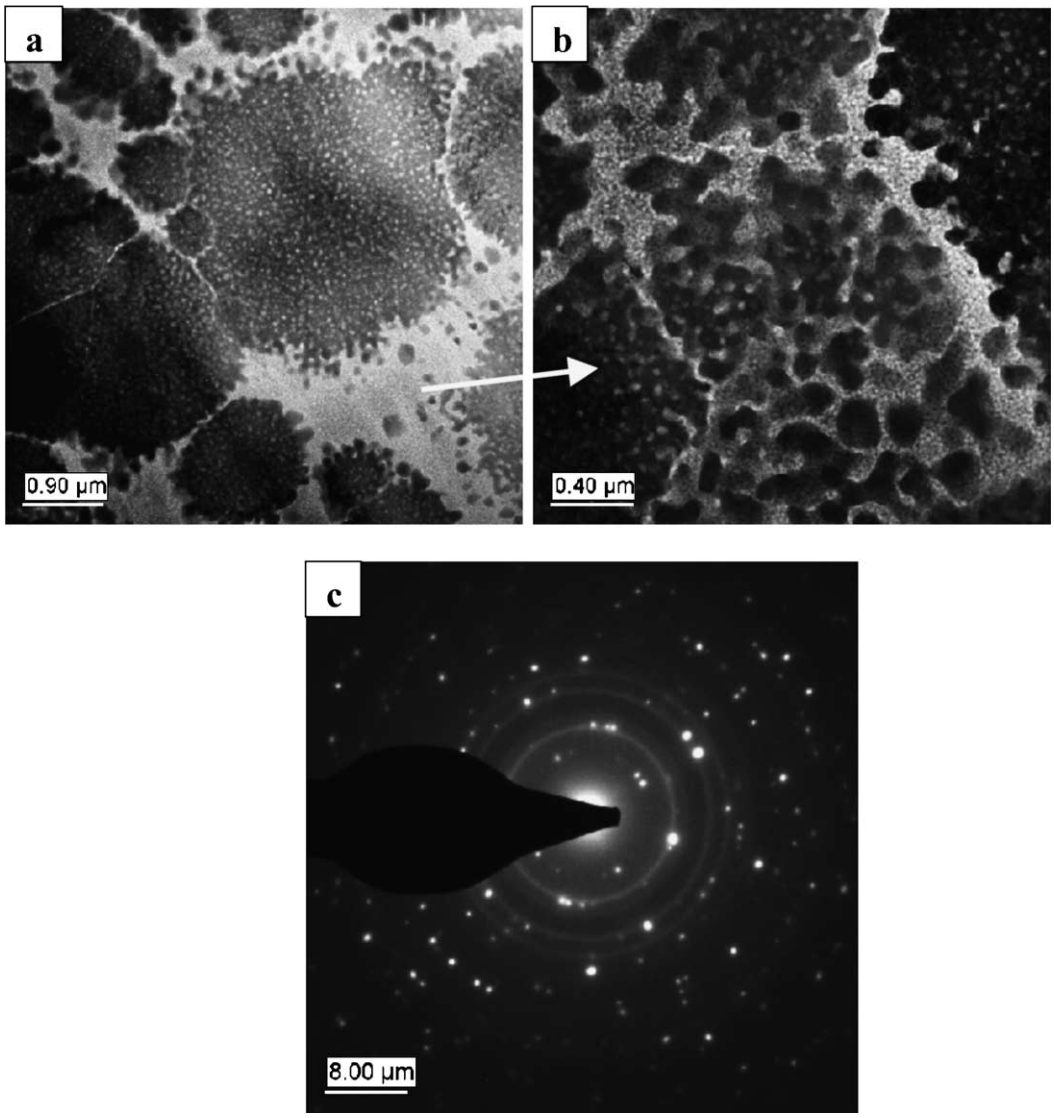

Fig. 3. TEM micrographs and SAED pattern of the PMN–PZ–PT film annealed at 800 °C.

is likely to relax the stress in some manner and allow for the creation of crack-free thin films, which is preferred in many applications to improve adhesion and minimized delamination. The distinguished porous phase has been clearly detected through higher magnification of the area (Fig. 3(b)). The perceived porous phase (at low magnifications) is actually comprised of a loose grain structure (verified by high magnification). The platinum substrate is a powerful nucleation agent, but crystallization retards densification, particularly when crystal growth is rapid enough so as to trap pores within crystal grains.[18–20] The PMN–PZ–PT system, in thin film form, seems to transform quickly enough that crystallization is complete before the porosity is removed. Fig. 3(c) shows the selected area electron diffraction (SAED) pattern from a small region. The interplanar spacings (d_{hkl}) observed from TEM and XRD data are very much comparable (Table 1), confirming the presence of a perovskite crystalline structure in the material.[21]

Fig. 4 shows the AFM surface topography of the PMN–PZ–PT films. The root mean square (rms) roughness values for the films annealed at 700, 800, and 850 °C vary slightly, and are around 7.7, 6.5, and 7.2 nm, respectively.

3.3. SIMS depth profile analysis

Fig. 5(a) and (b) presents the SIMS depth profiles around the interface between the PMN–PZ–PT films and their substrates. Comparing Fig. 5(a) profile curves of Pt, Ti, Zr, Mg, Nb, Pb, and Si with Fig. 5(b), which has diffusive tails that drop with a lower slope at the interface with Pt, indicates significantly enhanced interdiffusion between PMN–PZ–PT and Pt occurs when the temperature is increased from 800 to 850 °C. In addition, remarkable bumps are observed in the profiles of Ti, Zr, Mg, Nb, and Pb near the interface with Pt in the PMN–PZ–PT films annealed at 850 °C (Fig. 5(b)), but not in the films annealed at 800 °C (Fig. 5(a)). We

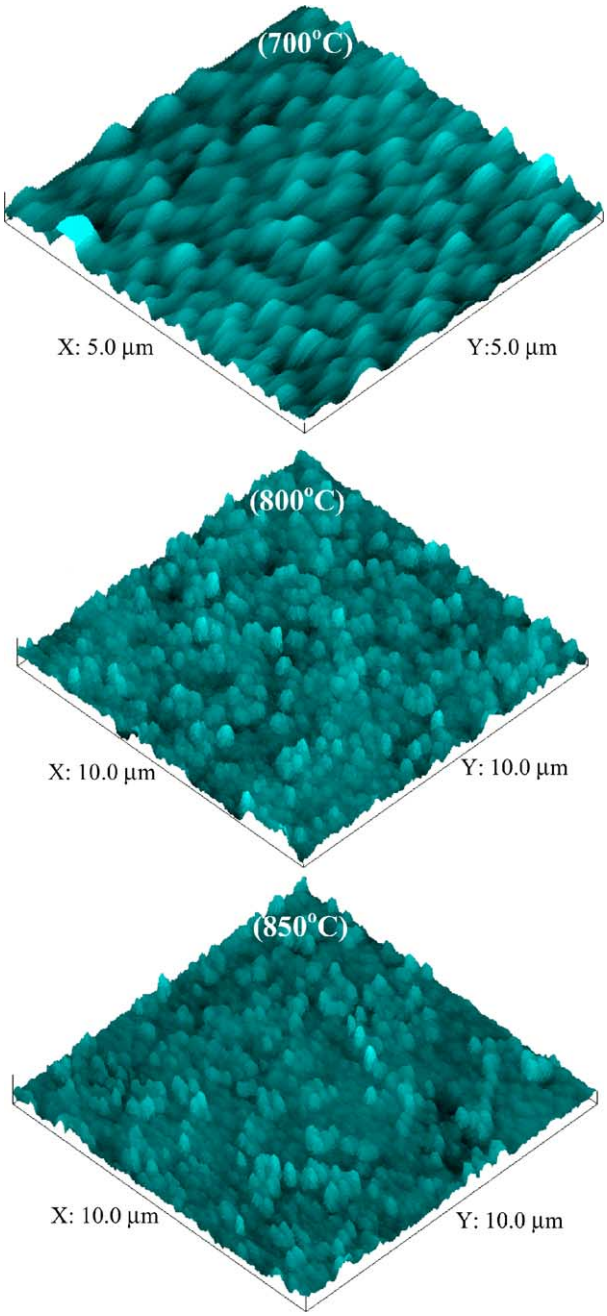

Fig. 4. AFM topography of the PMN–PZ–PT films annealed at different temperatures.

think the observed bumpy region in the 850 °C annealed films is significantly affected by the interdiffusion between PMN–PZ–PT and Pt. The existence of such a diffusion-affected region may be one of the reasons for the increased leakage current and reduced dielectric constant for the films annealed at 850 °C, compared with those at 800 °C.

3.4. Electrical characterizations

The results of the calculated leakage current density are shown in Fig. 6. It was observed that the leakage current is

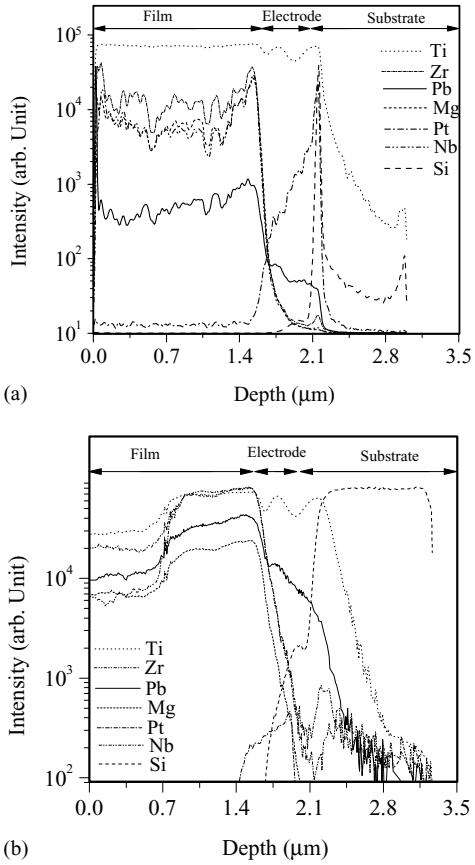

Fig. 5. SIMS depth profiles of the PMN–PZ–PT film annealed at 800 and 850°C corresponding to the figures (a) and (b).

reduced when the annealing temperature is increased from 700 to 800 °C. However, annealing beyond 850 °C led to a rise in leakage current that is probably caused by the formation of the interdiffusion regions in the film near the interface with Pt, as shown in SIMS.

The variation of the dielectric constant (ε) and loss (D) of the PMN–PZ–PT films annealed at different temperatures is shown in Fig. 7. With the increase of annealing tempera-

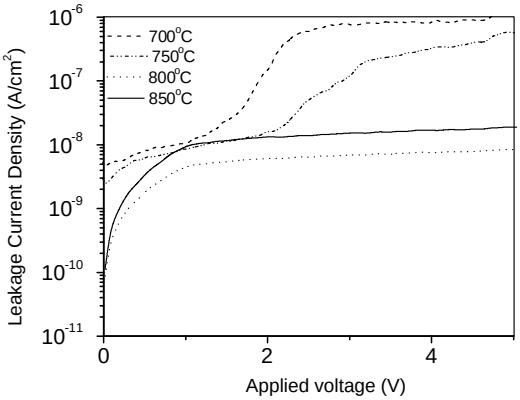

Fig. 6. The current–voltage (I–V) characteristics of the PMN–PZ–PT films annealed at different temperatures.

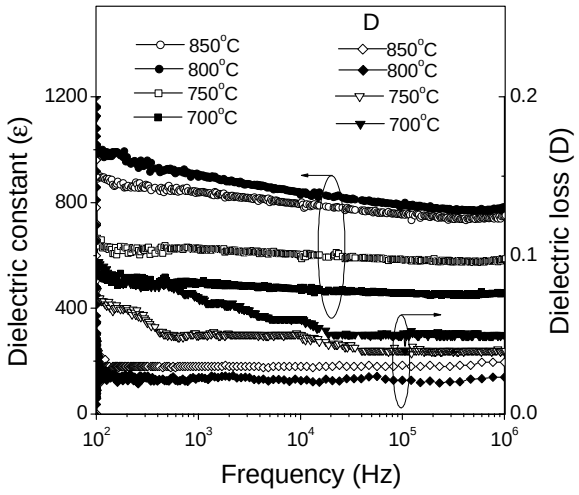

Fig. 7. Variations of dielectric constant and loss of the PMN–PZ–PT films with frequency at room temperature.

ture from 700 to 800 °C, the dielectric constant is increased due to the improved crystallization, as evident from our XRD results. The dielectric loss is reduced with increasing the annealing temperature below 800 °C, which is coherent with the reduction tendency of the leakage current. However, the dielectric properties trend to degrade (reduced dielectric constant and increased dielectric loss) upon elevating the temperature to 850 °C. This is believed to be caused by the formation of the interdiffusion layer and the Pb-deficient pyrochlore phase at this temperature, as detected with our XRD and SIMS experiments, respectively. The highest dielectric constant, 920 at 1 kHz, was observed for the films annealed at 800 °C, which is relatively low compared to PMN–PZ–PT-based bulk ceramics (∼1300 °C at 1 kHz). A possible reason may be the existence of pores in the films, as shown by our TEM images (Fig. 3(a) and (b)).[22]

Fig. 8 shows the polarization electric field (*P–E*) hysteresis loops of the PMN–PZ–PT films. With grain growth in the films, the remnant polarization is improved as the temperature increased from 700 to 800 °C. The remnant polarization

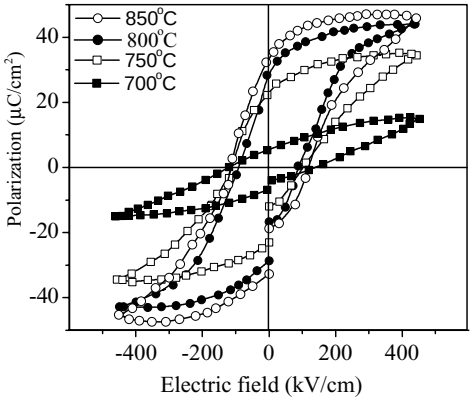

Fig. 8. The *P–E* hysteresis loops observed at room temperature for the PMN–PZ–PT films annealed at different temperatures.

(P_r) and coercive field (E_c) attained a value of 28 μC cm^{-2} and 91 kV cm^{-1}, respectively, for the film annealed at 800 °C compared with 25.34 μC cm^{-2} and 6.31 kV cm^{-1}, respectively, for bulk ceramics. No such data has been reported in the literature for similar PMN–PZ–PT films. For the sample annealed at 850 °C, the hysteresis loop becomes broader due to the increased leakage current.[23]

4. Conclusion

Perovskite 0.15PMN–0.45PZ–0.40PT (PMN–PZ–PT) thin films were prepared on Pt-coated Si substrates through a sol–gel process. XRD analysis confirmed the tetragonal symmetry in the films, and the interplanar spacings were calculated from both XRD and SAED results. Morphology and microstructures of the studied thin films were found to be sensitive to the annealing temperature, and the electrical properties were strongly determined by the morphology and microstructure. The films annealed at 800 °C for 1 min exhibited a high degree of crystallization with a pyrochlore free perovskite phase, along with optimized ferroelectric and dielectric properties. Annealing at a higher temperature (850 °C) resulted in serious interdiffusion at the interface between the film and the electrode layers, and the formation of the Pb-deficient pyrochlore phase substantially deteriorated the electrical properties.

Acknowledgements

The authors would like to thank Ms. Chow Shue Yin, Ms. Lai Mei Ying, Doreen and Dr. S. Tripathy for their assistance to carry out the work and helpful discussions.

References

1. Park, S. E. and Shrout, T. R., Ultrahigh strain and piezoelectric behavior in relaxor based ferroelectric single crystals. *J. Appl. Phys.* 1997, **82**, 1804–1811.
2. Sommer, R., Yushin, N. K. and van der Klink, J. J., Polar metastability and an electric-field-induced phase transition in the disordered perovskite $Pb(Mg_{1/3}Nb_{2/3})O_3$. *Phys. Rev. B* 1993, **48**, 13230–13237.
3. Tantigate, C., Lee, J. and Safari, A., Processing and properties of $Pb(Mg_{1/3}Nb_{2/3})O_3$–$PbTiO_3$ thin films by pulsed laser deposition. *Appl. Phys. Lett.* 1995, **66**, 1611–1613.
4. Nagarajan, V., Alpay, S. P., Ganpule, C. S., Nagaraj, B. K., Aggarwal, S., Williams, E. D. *et al.*, Role of substrate on the dielectric and piezoelectric behavior of epitaxial lead magnesium niobate–lead titanate relaxor thin films. *Appl. Phys. Lett.* 2000, **77**, 438–440.
5. Lee, J. K., Park, D., Cheong, D. S., Park, J. W. and Park, C. S., Phase development of radio-frequency magnetron sputter-deposited $Pb(Mg_{1/3}Nb_{2/3})O_3$–$PbTiO_3$ (90/10) thin films. *J. Vac. Sci. Technol. A* 2000, **18**, 1659–1662.
6. Stringfellow, S. B., Gupta, S., Shaw, C., Alcock, J. R. and Whatmore, R. W., Electrical conductivity control in uranium-doped $PbZrO_3$–$PbTiO_3$–$Pb(Mg_{1/3}Nb_{2/3})O_3$ pyroelectric ceramics. *J. Eur. Ceram. Soc.* 2002, **22**, 573–578.

7. Bove, T., Wolny, W., Ringgaard, E. and Pedersen, A., New piezoelectric PZT–PNN material for medical diagnostics applications. *J. Eur. Ceram. Soc.* 2001, **21**, 1469–1472.
8. Stemmer, S., Bai, G. R., Browning, N. D. and Srieffert, S. K., Microstructure of epitaxial $Pb(Mg_{1/3}Nb_{2/3})O_3$–$PbTiO_3$ thin films grown by metalorganic chemical vapor deposition. *J. Appl. Phys.* 2000, **87**, 3526–3531.
9. Yi, G., Wu, Z. and Sayer, M., Preparation of $Pb(Zr,Ti)O_3$ thin films by sol gel processing: electrical, optical, and electro-optic properties. *J. Appl. Phys.* 1988, **64**, 2717–2724.
10. Shannigrahi, S. R. and Jang, H. M., Fatigue-free lead zirconate titanate-based capacitors for nonvolatile memories. *Appl. Phys. Lett.* 2001, **79**, 1051–1053.
11. Bellaiche, L. and Vanderbilt, D., Intrinsic piezoelectric response in perovskite alloys: PMN–PT versus PZT. *Phys. Rev. Lett.* 1999, **83**, 1347–1350.
12. Shaw, J. C., Liu, K. S. and Lin, I. N., Piezoelectric properties of hot-pressed 18PMN–41PZ–41PT ceramics. *J. Mater. Sci.* 1993, **28**, 3335–3340.
13. Shaw, J. C., Liu, K. S. and Lin, I. N., Dielectric behavior at morphotropic phase-boundary for PMN–PZT ceramics. *Scripta Metal.* 1993, **29**, 981–986.
14. Shaw, J. C., Liu, K. S. and Lin, I. N., Modification of piezoelectric characteristics of the $Pb(Mg,Nb)O_3$–$PbZrO_3$–$PbTiO_3$ ternary-system by aliovalent additives. *J. Am. Ceram. Soc.* 1995, **78**, 178–182.
15. Miyashita, S., Shinozuka, M., Sumi, K., Muraj, M. and Takahashi, T., US Patent No. 6140746, 31 October 2000.
16. Norga, G. J., Vasiliu, F., Fè, L., Wouters, D. J. and van der Biest, O., Role of fluorite phase formation in the texture selection of sol–gel prepared $Pb(Zr_{1-x},Ti_x)O_3$ films on Pt electrode layers. *J. Mater. Res.* 2003, **18**, 1232–1238.
17. POWD, *An Interactive Powder Diffraction Data Interpretation and Indexing Program, ver. 2.1*, Wu, E. School of Physical Science, Flinders University of South Australia Bedford Park, S.A. 5042, Australia.
18. Park, J. H., Kang, D. H. and Yoon, K. H., Effects of heating profiles on the orientation and dielectric properties of $0.5Pb(Mg_{1/3}Nb_{2/3})O_3$–$0.5PbTiO_3$ thin films by chemical solution deposition. *J. Am. Ceram. Soc.* 1999, **82**, 2116–2120.
19. Liu, Y. M. and Phule, P. P., Nucleation-controlled or growth-controlled orientation development in chemically derived ferroelectric lead zirconate titanate ($Pb(Zr_xTi_{1-x})O_3$, $x = 0.4$) thin films. *J. Am. Ceram. Soc.* 1996, **79**, 495–498.
20. Tani, T., Xu, Z. and Payne, D. A., Preferred orientations for sol–gel derived PLZT thin layers. *Mater. Res. Soc. Symp. Proc.* 1993, **310**, 269–274.
21. Akbas, M. A. and Lee, W. E., Characterisation and densification of PLZT powder coprecipitated from chloride-nitrate solutions. *Br. Ceram. Trans.* 1996, **95**, 49–52.
22. Park, J. H. and Trolier-McKinstry, S., Dependence of dielectric and piezoelectric properties on film thickness for highly {1 0 0}-oriented lead magnesium niobate–lead titanate (70/30) thin films. *J. Mater. Res.* 2001, **16**, 268–275.
23. Moulson, A. J. and Herbet, J. M., *Electroceramic*. Chapman and Hall, 1990.